Physics of Fluids

Influence of wetting behavior on the morphology of droplet impacts onto dry-patterned micro-structured surfaces

Cite as: Phys. Fluids **34**, 123322 (2022); https://doi.org/10.1063/5.0124692
Submitted: 07 September 2022 • Accepted: 23 November 2022 • Published Online: 12 December 2022

P. Foltyn, D. Ribeiro, A. Silva, et al.

Physics of Fluids ARTICLE scitation.org/journal/phf

Influence of wetting behavior on the morphology of droplet impacts onto dry-patterned micro-structured surfaces

Cite as: Phys. Fluids **34**, 123322 (2022); doi: 10.1063/5.0124692
Submitted: 7 September 2022 · Accepted: 23 November 2022 ·
Published Online: 12 December 2022

View Online Export Citation CrossMark

P. Foltyn,[1,a)] D. Ribeiro,[2] A. Silva,[2] G. Lamanna,[1] and B. Weigand[1]

AFFILIATIONS

[1]Institute of Aerospace Thermodynamics, University of Stuttgart, Stuttgart, Germany
[2]AEROG-LAETA, University of Beira Interior, Covilhã, Portugal

[a)]Author to whom correspondence should be addressed: patrick.foltyn@itlr.uni-stuttgart.de

ABSTRACT

The influence of surface roughness, especially regularly patterned micro-structures on the physical outcomes of droplet impacts, is far from fully understood. In order to get a deeper insight into the physics of the impact phenomena, a systematic experimental study of the morphology on regularly patterned micro-structured surfaces has been carried out. The used structures with different dimensions were grooves and pillars with a square cross section. With the help of plasma activation and plasma polymerization processes, the surface wettability was modified independently from the surface structure and material. Two different test fluids were used, namely, distilled water and isopropanol, impacting with various impact energies onto the patterned surface samples. For a better characterization of the impact process, high-speed images from three different perspectives have been acquired synchronously. Due to the transparent surface material, the bottom perspective using a total internal reflection configuration was able to visualize air entrapment inside the surface structure. To the authors' knowledge, such images are not available in the literature, yet. The outcomes have been qualitatively investigated, summarized, and compared. A dependency of the outcomes on the impact energy, the surface wettability, and the structure dimensions could be clearly shown. In general, increasing impact energy will promote the tendency of splashing. However, roughness features cannot only trigger splashing, but can also inhibit it, for example, crown splashing. Moreover, reproducible arrangements of air entrapment inside the structure could be found, which was addressed by the authors as "cookie" and "button" due to their appearance.

I. INTRODUCTION

Surface roughness and wettability have a significant influence on the physical processes of droplet impacts onto dry walls by Yarin *et al.*[1] The publication of Rioboo *et al.*[2] investigated the influence of surface wettability and surface roughness for $R_a < 25.6\mu$m, where R_a is the arithmetic mean roughness.[3] They found that the roughness has a strong influence on the prompt splash limit. The presence of roughness as well as an increasing magnitude of surface roughness is significantly promoting the splashing behavior.[4,5] Josserand *et al.*[6] could experimentally and numerically trigger the occurrence of splashing with rough obstacles. Based on experiments, several correlations for the splashing limit have been developed.[5,7,8] Additionally, Antonini *et al.*[9] could show that the maximum spreading ratio and the time scales of the different spreading regimes are subject to changes depending on the advancing and receding contact angles, surface roughness, impact energy, and physical liquid properties. These findings were supported by the experiments of Stow and Hadfield[10] and Range and Feuillebois.[11] Both showed that the description and prediction of splashing are not only dependent upon the mean roughness R_a but also upon other characteristics, such as surface material, and hence indirectly, surface wettability. As Papierowska *et al.*[12] pointed out, roughness and wettability are closely related, when it comes to the description of the droplet impact outcome. This concerns the basic phenomenon as well as the spreading diameters and velocity of ejected droplets.

In all previously mentioned papers, the surfaces were randomly (isotropic) rough, which might come either from the natural shape (e.g., wood[13] or leaves[12]), the general production method (e.g., glass[14]), or special treatment (e.g., chemical treatment, coating,[9] sandblasting or sandpaper[11,14]). Moreover, the wettability was never modified independently from the surface roughness and topography, respectively. In previous studies, the change of wettability was

mainly achieved by exchanging the complete surface itself and thus also the surface material.

Splashing investigations on regularly structured surfaces having pillars with a square cross section or grooves exhibit an inherently different behavior from surfaces with isotropic roughness, just due to the structure itself. When using regular structured surfaces, droplet impacts can show a droplet spreading into preferential directions along the structure orientation.[15–18] Concerning the splashing phenomenology, the arrangement of the structure elements influences the splashing direction.[19] The splash at one single structure item could be triggered in experiments conducted by Josserand *et al.*[6] Furthermore, Ren *et al.*[20] showed that the flow field around this element features air entrapment dependent on the local impact point with respect to the element position. Looking at a field of structure elements, prompt splashing can be significantly promoted and the magnitude controlled by the structure height.[21] The air entrapment in between the structure can be considered here as one of the driving mechanisms for the splashing behavior since an increase in the distance between the roughness elements can suppress splashing and, therefore, increase the critical Weber number.[19]

In addition, by manipulating the wettability, for example, the direction of rebounding droplets is controllable. Malouin *et al.*[22] and Yada *et al.*[23] have achieved this so-called "droplet vectoring" by a non-uniform wetting behavior due to a non-uniform texture. Yet, also for uniform textures, as the results will show in this article, the wetting behavior will have a substantial influence on the droplet impact phenomena.

Considering the available literature, the present paper shall address the following questions. How is the impact morphology, for example, directional splashing and spreading, influenced by a regularly patterned micro-structure and different wettabilities? What are the driving phenomena of secondary droplet production during splashing as well as during the receding phase? What factors does air entrapment depend on during the droplet impact, especially in regard to structure dimensions and surface wettability?

Therefore, the droplet impact morphologies with different impact conditions on dry, regularly structured surfaces are systematically investigated. Hereby, the droplet liquid, the surface structure, the surface wettability, and the surface material are flexibly altered independently to get a deeper insight into the underlying physical processes. In particular, the independent modification of the wettability using plasma processes without changing the surface material and consequently also the characteristic surface roughness is one of the major novelties in our approach. A special focus is set on the splashing limit, the bubble entrapment, and the impact morphology under the consideration of the surface structure and wettability. Therefore, an experimental facility has been used providing three different perspectives:[24] diffuse backlight images of the lateral and top perspectives, and the bottom perspective in a total internal reflection configuration.[25–27] The latter perspective is very rarely reported in the literature, but allows a distinction between wetted and non-wetted areas inside the structures and the tracking of air entrapment. As structures, three different structured fields with equidistant pillars with a square cross section and one field of grooves were investigated. The surface samples were made of two different surface materials, Lexan® (polycarbonate, PC) and Plexiglas® [poly(methyl methacrylate), PMMA] of which the wetting behavior could be flexibly modified using plasma activation and plasma polymerization. As droplet fluid, distilled water and isopropanol (2-propanol) had been used. In releasing the droplets from four different falling heights, the impact energy could be controlled resulting in a wide range of Weber and Reynolds numbers at impact conditions, $80 < We < 1165$ and $1135 < Re < 12\,240$. The Weber and Reynolds numbers based on the droplet impact velocity u, the droplet diameter D, the fluid density ρ, the viscosity μ, and the surface tension γ are defined as follows:[28]

$$Re = \frac{\rho u D}{\mu}, \tag{1}$$

$$We = \frac{\rho u^2 D}{\gamma}. \tag{2}$$

II. INVESTIGATED MICRO-STRUCTURED SURFACES

To be able to observe heterogeneous wetting states and air entrapment using the total internal reflection configuration, which is further explained in Sec. IV A, the surface materials were chosen to be transparent PC and PMMA. The structured patterns have been chosen to be micro-metric grooves and pillars with the dimensions depicted in Fig. 1 and summarized in Table I. The height of all used structures is $h = 20\mu$m. The grooves ($S1$), see Fig. 1(a), are namely very long pillars with a width of $w_1 = 60\mu$m and a length of $w_2 = 500\mu$m. The orthogonal distance of each groove is $d_1 = 60\mu$m, while the gap of $d_2 = 15\mu$m, into the direction of the grooves, is due to manufacturing reasons of the hot embossing procedure. The pillars with a square cross section ($S2 - S4$), see Fig. 1(b), have an edge length and a gap between each other of $w = d = \{60; 30; 15\mu\text{m}\}$. Further parameters describing the topography of the different structures can be also found in Table I: the surface roughness parameters R_a, R_z, and R_{sm}, the

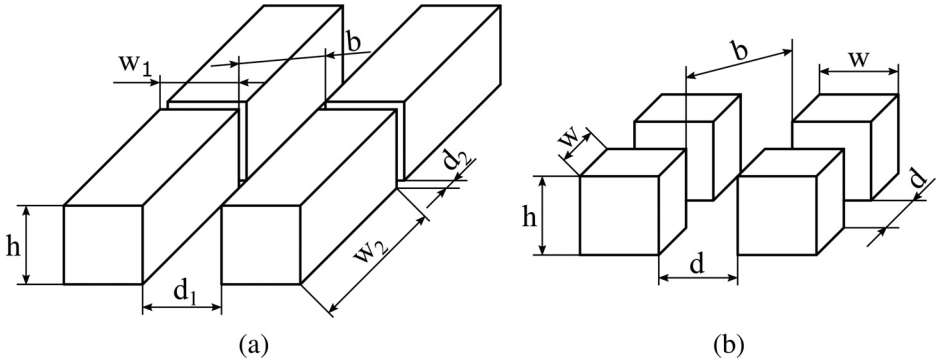

FIG. 1. Dimensions of the used structured surfaces: (a) grooves ($S1$), (b) pillars with a square cross section ($S2 - S4$). The respective dimensions are summarized in Table I.

TABLE I. Overview of the dimensions of used micro-structured surfaces and the respective topography parameters, which are further described in Sec. V A and are used then for the evaluation. *S*1 corresponds to grooves, see Fig. 1(a); *S*2 − *S*4 correspond to pillars with a square cross section, see Fig. 1(b). R_a and R_z are correspond to calculated roughnesses, r is the roughness factor according to Wenzel,[29] and α is the topography parameter introduced by Tsai *et al.*[19] for describing regularly structured surfaces. The authors have chosen to modify this parameter as $\alpha_{mod} = b/h$. Herein, the diagonal b of the spacing between the individual structure elements is used.

		Dimensions [μm]			Topography parameters					
ID	Type	Edge length	Distance	Height	$R_a[\mu m]$	$R_z[\mu m]$	r	α	α_{mod}	$b[\mu m]$
*S*1	Grooves	$w_1 = 60$, $w_2 = 500$	$d_1 = 60$, $d_2 = 15$	$h = 20$	10	20	1.36	1.0	3.1	61.85
*S*2	Square pillar	$w = 60$	$d = 60$	$h = 20$	7.5	20	1.33	1.4	4.2	84.85
*S*3	Square pillar	$w = 30$	$d = 30$	$h = 20$	7.5	20	1.67	1.4	2.1	42.43
*S*4	Square pillar	$w = 15$	$d = 15$	$h = 20$	7.5	20	2.33	1.4	1.1	21.21

Wenzel factor r, and the parameter α for describing the gaps in relation to the width introduced by Tsai *et al.*[19] using the diagonal distance b of the junctions. Additionally, a modified α_{mod} has been used in order to describe these gaps in a three-dimensional way. The definition of these parameters and the interpretation of the results using them can be found in detail in Sec. V.

The surface specimens have been manufactured in a three-step procedure, which is a combination of LASER lithography, nickel electroforming, and hot embossing.[30,31] The reproduction quality of the surface samples is very high and was carried out at the *Karlsruhe Nano and Micro Facility (KNMF), Germany*. By means of scanning electron microscopy (SEM), micro-computed tomography (microCT), and classical optical microscopy, an initial quality check was done as well as interval checks. Figure 2 shows exemplary SEM images of the respective surfaces.

At the beginning of our study, we were not sure if the droplet impacts will damage the micro-structures. Thus, the samples were closely examined under the microscope and mapped after each impact to observe whether the pillars are damaged. However, no defects or changes could be detected. Therefore, it can be concluded that the drop impact does not damage or destroy the surface structure for the tested cases and long-term durability is ensured.

III. WETTING BEHAVIOR ON STRUCTURED SURFACES AND ITS MODIFICATION

Droplet impacts on surfaces with varying wetting behavior have been investigated. To be able to characterize the latter, the sessile drop method was used. For this measurement task, an optical contour analysis (OCA) of *DataPhysics Instruments GmbH* was used. It consists of a camera mounted to a far-field microscope, a precise syringe pump, a height-adjustable table, and a diffuse backlight. During the measurement, a 5 μl droplet of the respective droplet liquid was generated making it hang on the tip of a blunt needle. The height-adjustable table was moved up in order to gently place the droplet on the surface avoiding any influence onto the apparent contact angle θ_{app}. The contour of the droplet was then fitted by ellipses, and the arithmetic mean contact angle at the left and right triple points was used as apparent contact angle. This procedure was repeated several times at several spots in order to minimize the influence of local inhomogeneities in the free surface energies. As shown in the literature,[31] the definition and measurement of contact angles on structured surfaces is very challenging. On regularly structured surfaces, a contact angle range with a variance of several degrees up to several tens of degrees can be observed. The used untreated surface samples made of PC for the droplet impact show a variance in the contact angle of approximately 15° for the pillars with a square cross section (*S*2 − *S*4) to 43° for grooves (*S*1).[31] Therefore, each structured surface specimen had its smooth "partner sample," which is treated in the same way as the structured sample. The contact angle was measured on the partner sample in order to classify the wetting behavior into the wetting intervals of Table II. The modification of the wetting behavior has been carried out, again, using plasma activation and plasma polymerization using *Femto* plasma machines by *Diener electronic GmbH & Co KG*. Since the structured surface samples could not be trashed after each experiment, they had to be cleaned within the general procedure described in Sec. IV B and reused. The same cleaning procedure was, therefore, also applied to the smooth partner sample in order to maintain the consistency of the material properties.

IV. EXPERIMENTAL APPROACH

In the following, the experimental test rig is briefly outlined. Then, the experimental procedure will follow, and finally, the parameter space will be introduced.

A. Experimental test rig

The experimental test rig can be used for droplet impacts on various surface types, as long as the surface material is transparent. The surfaces can have micro-structured patterns, as presented here, or they can be also smooth.[24] It consists mainly of three units: a droplet generation unit, an image acquisition unit, and a triggering and synchronization unit. For a better description, a coordinate system is introduced which corresponds to the droplet impact point, see Fig. 3.

1. Droplet generation unit

The droplet generation is realized by using a syringe pump, which is connected to a blunt needle with an outer diameter of 0.4 mm. To avoid any chemical interaction, Teflon® tubes and glass syringes were used. The needle was tilted by 45° in order to ensure a defined droplet detachment and a more deterministic falling trajectory. Included backflow valves prevent air inside the tubing system so that a homogeneous droplet chain with constant droplet sizes could be established. From this droplet chain, one random droplet was selected for each impact experiment to pass the droplet barrier and impact

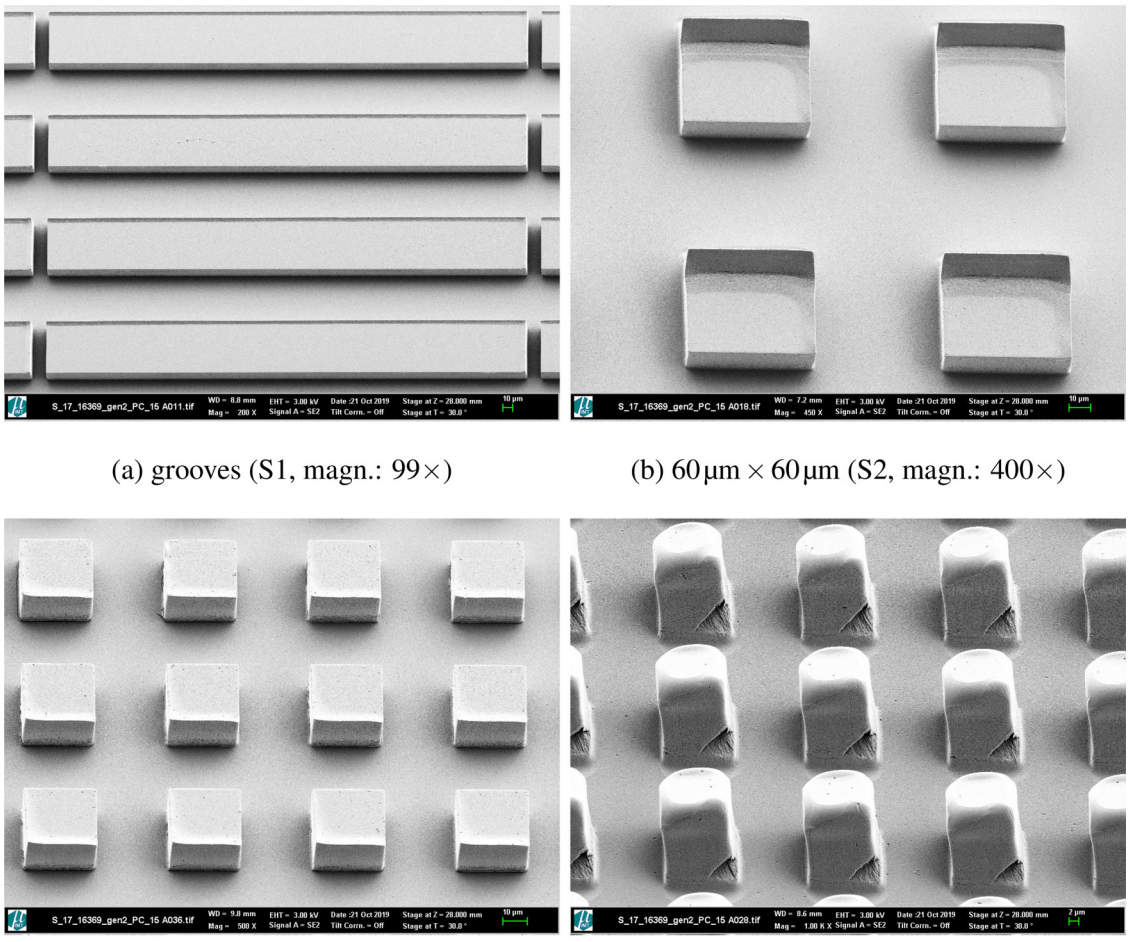

(a) grooves (S1, magn.: 99×) (b) 60 µm × 60 µm (S2, magn.: 400×)

(c) 30 µm × 30 µm (S3, magn.: 300×) (d) 15 µm × 15 µm (S4, magn.: 500×)

FIG. 2. Micro-structured Lexan® surfaces of different dimensions acquired with scanning electron microscopy (SEM). The magnification of each image is given at the respective image. The specimen stage was tilted by 30°: (a) grooves (S1), (b) 60 × 60 μm^2 pillars (S2), (c) 30 × 30 μm^2 pillars (S3), and (d) 15 × 15 μm^2 pillars (S4). From Foltyn *et al.*, *Droplet Interactions and Spray Processes*. Copyright 2020 Springer Nature. Reprinted by permission from Springer Nature.[30]

TABLE II. Summary of the evaluated parameters using the physical properties of Table III. For each column, the indicated parameter range was investigated. The parameters, which are requiring a pretreatment by plasma activation or polymerization, are marked. Data are partially extracted from Ref. 24.

Liquid		Distilled water				Isopropanol			
Material		PC		PMMA		PC		PMMA	
Contact angle		0°∗		0°∗		0°		0°	
		25°–40°∗		25°–40°∗					
		79.8°		75.1°		66°–73°⋆		66°–73°⋆	
		117°–122°⋆		117°–122°⋆					
Impact conditions	Re:	4130	6860	9360	12 240	1135	1745	2315	2955
	We:	80	205	385	665	165	400	715	1165
Surface structure		Surfaces: *S*1 − *S*4, see Table I				Surfaces: *S*1 − *S*4, see Table I			
Plasma treatments		The used samples were treated by plasma activation (∗) and plasma polymerization (⋆)							

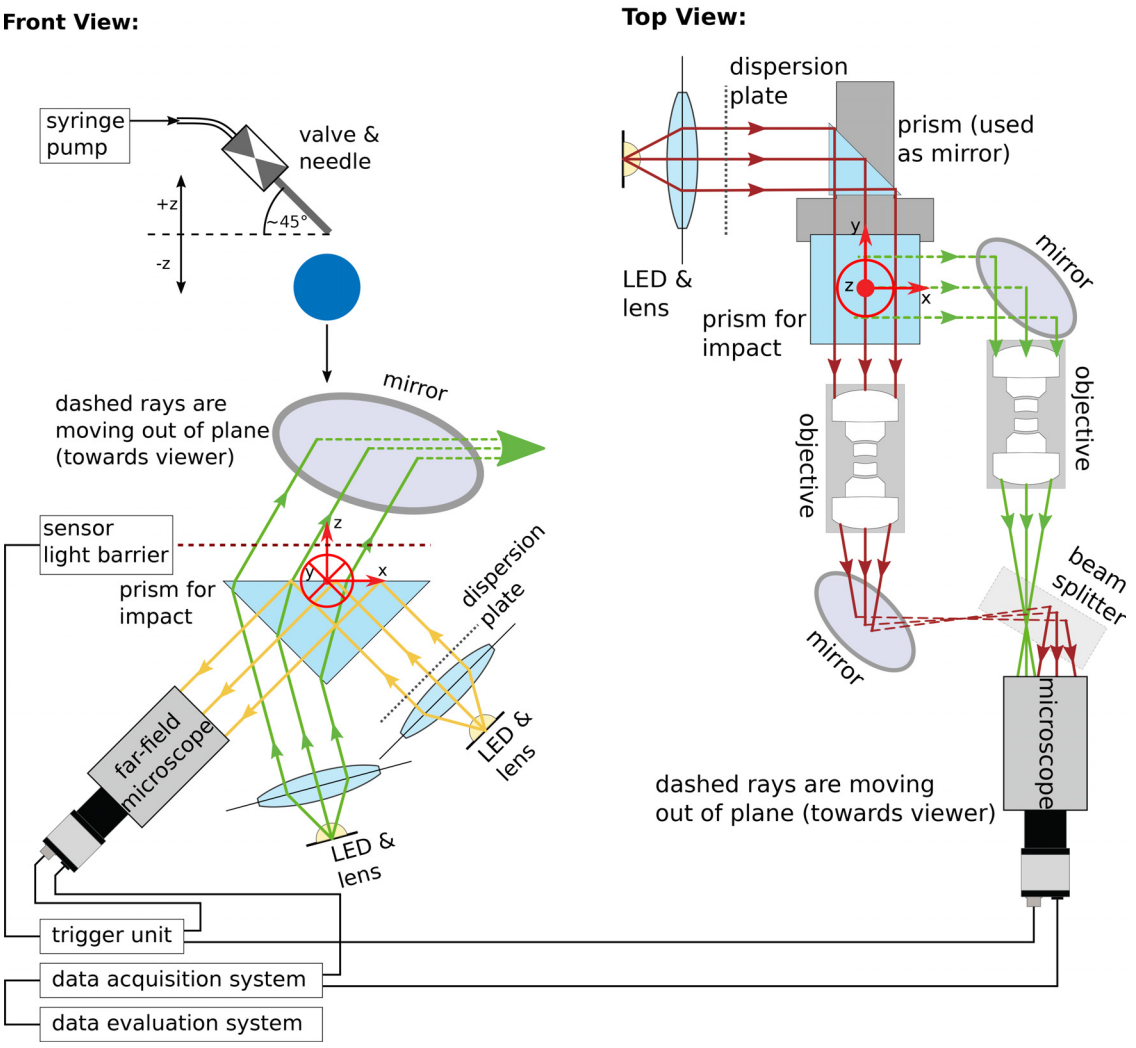

FIG. 3. Schematic sketch of the image acquisition unit—left side: front view, right side: top view. The different colors indicate the different light paths, yellow for bottom perspective, green for top perspective, and red for lateral perspective. Dashed light paths emerge from the sketch plane. The droplet impact point is marked by the given coordinate system. Reproduced from Foltyn *et al.*, Phys. Fluids **33**, 063305 (2021) with the permission of AIP Publishing LLC.[24]

onto the surface specimens. Different impact velocities were set in changing the falling height of the droplet.

2. Image acquisition unit

The image acquisition unit consists of three different synchronized perspectives:[24] a bottom perspective in a total internal reflection configuration,[25–27,32] a top perspective, and a lateral perspective with a spatial resolution of 17.0, 18.1, and 28.8 μm, respectively. The optical concept of the respective perspectives is shown in Fig. 3 with different colors. In total, two *Photron SA-X2* high-speed cameras at a resolution of $1024 \times 672\text{px}^2$, a frame rate of 20 000 fps, and a shutter time of 1/88888 s have been used. During the post-processing, for each perspective, an individual routine for correcting the perspective-related distortion errors has been applied at the beginning of any further image processing. All shown pictures in this paper are already corrected. In the following, each perspective is explained in detail.

a. Bottom perspective. For the bottom perspective, parallel light is generated using a *Cree XLamp XHP70 SMD* High-Power LED and an aspheric condenser lense.[24] It enters a rectangular prism at an angle of 45° in respect to the top surface, as depicted in the front view of Fig. 3. In the case of a dry surface and due to the occurring total internal reflection, the light is reflected, leaving the prism, and entering a *Navitar Zoom 6000* far-field microscope at which one high-speed camera is mounted. For this case, the camera is detecting a bright image, see Fig. 4(a). The critical angle of incidence ξ_{crit} in respect to the prism top surface can be calculated using Snell's law[33] and depends only on the refractive index relation n_i/n_j of adjacent layers

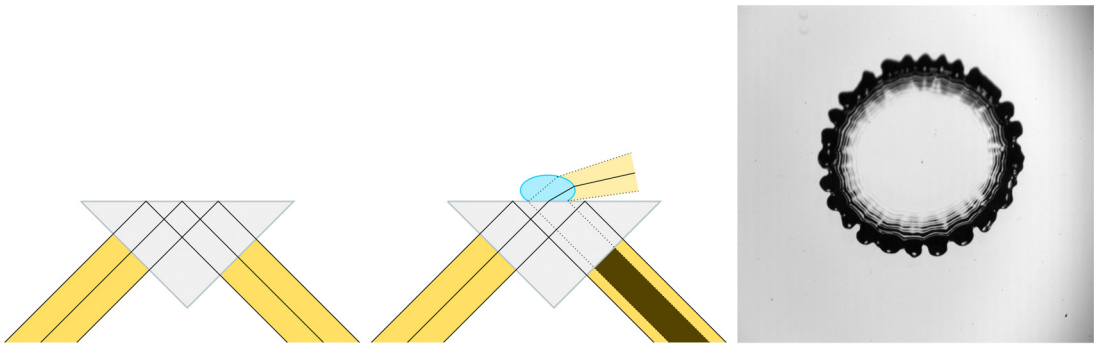

FIG. 4. Schematic of the total internal reflection configuration: (a) dry surface—all light rays are reflected at the upper surface, (b) wetted surface—light rays in area of wetted surface are not reflected anymore, (c) bottom perspective of a measurement showing wetted and dry areas. For sake of simplicity a smooth surface was used instead of a micro-structured surface. Reproduced from Foltyn *et al.*, Phys. Fluids **33**, 063305 (2021) with the permission of AIP Publishing LLC.[24]

$$\xi_{crit} = \arcsin n_2/n_1. \tag{3}$$

In the case of liquid at the top, the total internal reflection might not occur due to the fact that the angle of incidence is lower than the critical angle $\xi_{inc} < \xi_{crit}$. Two reasons might be possible. The liquid surface is either tilted, or the relation of the refractive indices has changed due to the different medium at the interface. As a result, dark spots can be detected by the camera for both cases, see Figs. 4(b) and 4(c). In case the liquid surface is horizontal, the camera might still detect bright spots for wetted areas, because this case is due to the parallel liquid and prism surface comparable to the dry case. Due to the topography of the droplet, these areas are, nevertheless, surrounded by a dark area because the surface needs to be tilted at a certain point, Fig. 4(c). Therefore, a clear and doubtless assignment of wetted areas is possible.

b. Top perspective. For the diffuse backlight images of the top perspective, parallel light is generated as depicted in the front view of Fig. 3. The light rays coming from the bottom of the prism are refracted by the prism and transverse the impact area to the mirror.[24] The mirror directs the images into the direction of the *WILD Heerbrugg M8* microscope and the high-speed camera (y direction), see top view of Fig. 3. Inside the microscope, the top and lateral perspectives are combined; however, the working distance of approximately 90 mm is too small for a simple combination. Therefore, two identical *Schneider Kreuznach Symmar 80/5.6* objectives are used for intermediate imaging enlarging the optical paths of the top and lateral perspectives by 320 mm so that a combination is possible. Before the rays enter the microscope and the prism, they are transmitted through a 50:50 beam splitter plate.

c. Lateral perspective. The lateral perspective is established using parallel light from a LED-lense system. The light is redirected by a small prism used as a mirror into y direction, see top view in Fig. 3. The arrangement was necessary due to the hardware periphery of the test rig. After traversing the droplet impact area, the light is going through the *Schneider Kreuznach Symmar 80/5.6* objective for intermediate imaging, as explained before for the top perspective. The combination of a mirror and a 50:50 beam splitter plate, used for this perspective as mirror, directs the lateral perspective into the microscope and onto the CMOS-chip of the high-speed camera.

3. Triggering and synchronization unit

For triggering the experimental setup, a light sheet is used. As the droplet cuts the light sheet, a TTL signal is sent to the "primary" camera. The primary camera acquires the top and lateral perspectives, which are combined on one CMOS-chip and thus are "optically" synchronized, as explained before. The primary camera passes the TTL signal as well as the frame rate and shutter speed to the "replica" camera. With the help of an oscilloscope at a sampling rate of 125 kHz, no measurable desynchronization for all frames was detectable.

B. Experimental procedure

The experimental procedure for drop impact experiments with micro-structured surfaces can be largely adopted from the procedure for experiments with smooth surfaces.[24] However, due to the high reproduction efforts, the micro-structured surface samples had to be reused after each experiment so that also an appropriate cleaning procedure was established. Furthermore, to each structured surface sample, a smooth surface sample was assigned as partner sample of the identical material. Each treatment, like plasma processes or cleaning, was done pairwise to maintain consistency.

As explained in Foltyn *et al.*,[24] the samples were cleaned, respectively, plasma treated if necessary, and placed on an isopropanol film on top of the prism surface. After setting the triggers of the camera, a random droplet was selected of the droplet stream to impact onto the structured surface sample, which was then recorded by all high-speed cameras when the light barrier was cut by the droplet. In addition to the general cleaning and to get the setup back to the initial state, the surface samples must be also returned to their original state. To do so, the droplet was removed from the structured surface using again the *PFA Nitrogen Gun*. Then, both the structured sample and its partner sample were put into a bath of liquid depending on the wetting behavior and the used droplet liquids. If isopropanol was used as droplet liquid, the samples were put for about ten minutes into an isopropanol

bath. If distilled water was used as droplet liquid and the wetting behavior was hydrophilic or superhydrophilic, respectively, the samples were flushed shortly with nitrogen and then placed into a bath of distilled water for about ten minutes. This was used in order to deactivate the surfaces before they were activated again. If distilled water was used as droplet liquid and the wetting behavior was hydrophobic, the surfaces have been directly placed into a bath of distilled water. Isopropanol was not used to avoid interactions with the coating, which might then have had a further influence on the subsequent experiments. A new plasma polymerization was not necessary, since the water droplet had, as expected, no influence on the coating and on the non-wetting properties.

After the experimental setup and the surfaces were set to the initial state, the procedure could start from the beginning. The structured surface samples have been checked for any developing damages and irregularities after finishing one experimental set of constant impact velocity. In general, it was very important to keep the time between the plasma processes and the droplet impact as short as possible to avoid any influence of the environment on the wetting behavior. For a short time, say in a range of several hours, the influence of the environment onto the degree of activation of the used PC and PMMA samples can be neglected.[40]

C. Investigated parameter space

The investigated parameter space is summarized in Table II using the liquid properties summarized in Table III. The structures were made of two different surface materials, which were Lexan® (polycarbonate, PC) and Plexiglas® [poly(methyl methacrylate), PMMA]. Distilled water and isopropanol (2-propanol) droplets with diameters of approximately (2.3 ± 0.1) mm and (1.9 ± 0.1)mm have impacted onto the surface samples. Depending on the liquid, different wetting behaviors could be investigated. For distilled water, four different contact angles were chosen. For the two most hydrophilic experimental cases, the surfaces have been plasma treated to achieve apparent contact angles of $\theta_{app} \approx 0°$ and in a range of $\theta_{app} \in [20°; 40°]$, which were lower than the natural apparent contact angle of water on PC and PMMA with $\theta_{app} = 79.8°$ and $\theta_{app} = 75.1°$, respectively. On the contrary, the hydrophobic surfaces have been plasma polymerized resulting in apparent contact angles between $\theta_{app} \in [117°; 122°]$. Using isopropanol droplets, only two different wetting behaviors were investigated since the natural behavior is already superhygrophilic ($\theta_{app} \approx 0°$). With the help of plasma polymerization, apparent contact angles in the range of $\theta_{app} \in [66°; 73°]$ could be achieved. For the impacts, four different impact energies, determinable by a variation in the falling height of the droplet, were used and resulting in the shown impact conditions in Table II as pairs of Reynolds and Weber numbers.

TABLE III. Summary of the fluid properties used for the experimental parameter study at an ambient temperature of 25 °C.

	Unit	Distilled water	Isopropanol (2-propanol)	References
Density ρ	kg m^{-3}	997.1	781.5	34 and 35
Surface tension γ	Nm^{-1}	0.071 98	0.020 92	36 and 37
Dyn. viscosity μ	mPa s	0.8897	2.045	38 and 39

V. RESULTS

In this section, the length scales, which characterize the micro-structured surfaces, will be presented and described. Then, the droplet spreading is further analyzed. Furthermore, the impact outcomes will be divided into deposition, splashing, and rebound, and a splashing limit will be investigated in dependency of the introduced length scales. Later, the different phenomena and their morphology will be described qualitatively and will be analyzed.

A. Length scales characterizing the micro-structured surfaces

There are many length scales to characterize the roughness of a target surface.[3,19,29] One of the most used is the arithmetical mean roughness, R_a, also called amplitude average roughness, which is defined as the mean absolute deviation of roughness irregularities from the centerline, defined by Eq. (4)

$$R_a = \frac{1}{l}\int_0^l |y(x)|\, dx, \tag{4}$$

where l is the length of the irregularity and y is the height from the mean line. In the present case, a volumetric approach was needed, and instead of a mean line, a mean plane was calculated. The value of R_a is the same for all square pillars, $R_a = 7.5\ \mu$m, since the height of the pillars is equal for all cases and the width of the pillars is equal to the space between them. On the other hand, for the surface composed of grooves, $R_a = 10\ \mu$m. The mean roughness itself is not enough to describe the surface topography.[41] Furthermore, in the recent study of Wang *et al.*,[42] it was confirmed that different definitions of roughness might lead to different results. Thus, another length scale is R_z, the mean of five individual values of distances between the highest peak and the deepest valley for five consecutive sample lengths.[3] Here, the R_z value is the same for all micro-structured surfaces tested, $R_z = 20\ \mu$m, corresponding to the roughness element height h.

Tsai *et al.*[19] studied the splashing mechanism of a droplet impinging on structured surfaces. They reported that the arrangement of the micropillars significantly affects the splashing morphology. This parameter $\alpha = b/w$ defines the ratio of the largest length scale of the cavity, which can be passed by air (b is the diagonal between two elements) related to the roughness element width in one micro-pattern unit (w). The value of α is equal for all the pillars with a square cross section, $S2 - S4$, $\alpha = 1.4$, and for $S1$, it is smaller, $\alpha = 1.0$. Tsai *et al.*[19] related the critical Weber number We_{crit} to the arrangement of pillars in a two-dimensional plane. It could be shown that, for the same parameters, different critical Weber numbers could be obtained. In addition, Xu[21] and Courbin *et al.*[43] concluded that splashing can be inhibited by increasing the pillar's height and surface roughness, respectively. Therefore, we decided to introduce a modified α, which is the ratio between b and the height of the pillars $\alpha_{mod} = b/h$ in order to account for the three-dimensional shape of the structure, analogous to the Wenzel factor approach, which will be described next.

In 1936, Wenzel[29] proposed the Wenzel equation for rough surfaces. He introduced the roughness factor r, which is the ratio between the actual surface area and the projected surface area. Thus, smooth surfaces have a value of $r = 1$ and rough surfaces of $r > 1$. Although the geometries of $S1$ and $S2$ are different, the roughness factors are almost the same. Regarding the pillars with a square cross section, r increases while decreasing the pillar width. All the length scales studied

in this work are given in Table I and will help to disclose the role of roughness on the droplet morphology dynamics.

B. Droplet spreading

This study is characterized by a wide range of impact conditions using different fluids, surface micro-patterns, surface materials, wettabilities, and impact energies. The droplet spreading phase is characterized by an increasing spreading diameter D_{spread}, while the receding phase shows a decreasing spreading diameter D_{spread}. As known from the literature,[2] the strength of the receding phase is strongly dependent on the surface wettability. During the spreading phase, different surface wettabilities show only an effect in the time range during where the inertial forces are not too dominant.[24,44] However, these findings were generated using smooth surfaces. The situation for regularly structured surfaces in the presented study is more complex.

For full-wetting smooth[24] or structured surfaces, a continuous spreading can be observed although the inertial forces have been completely dissipated. Moreover, also for contact angles of $\theta_{app} \leq 40°$ a continuous spreading could be observed, however, less significant as for $\theta_{app} \approx 0°$. In comparison, smooth surfaces at the same wettability already showed a very significant receding movement of the liquid front. The reason for this wicking is the capillary forces inside the surface structure. In consequence, the definition of a maximum spreading diameter for continuous spreading has been not possible. Therefore, only data with $\theta_{app} > 40°$ are compared for the maximum spreading diameter as the definition of a maximum spreading diameter has been only possible for such cases. In Fig. 5, the maximum spreading diameter normalized by the impact diameter $(D_{spread}/D_0)_{\max}$ is shown vs the dimensionless (inertial) time at which this maximum spreading diameter was reached $\tau[(D_{spread}/D_0)_{\max}]$. On the right graphic, the Wenzel factor r is shown. The spreading diameter has been averaged over the complete azimuthal angle range of 360°. The dimensionless (inertial) time is defined as $\tau = (tu_0)/D_0$ using the absolute time t, the droplet impact diameter D_0, and impact velocity u_0.

The scatter points represent hereby the arithmetic mean value for one experimental data set defined by one certain surface material, structure type, wettability, impact energy, and droplet fluid. As expected and already reported for smooth surfaces,[24] the spreading diameter is increasing with growing impact energy. Furthermore, the general trend shows that additionally the duration of the spreading process is also increasing. However, it is noticeable that some experiments of the two highest impact energies were reaching the maximum spreading faster. The respective experiments had larger structural items, that is, grooves and large pillars. The reason for this is an observable crown splashing. Therefore, the spreading liquid sheet is not interacting with the surface structure for most of the time and, thus, is able to spread faster than in the other cases. Important to notice is that the corresponding parameters are exclusively experiments with a contact angle of $\theta \in [66°; 80°]$. Only for this wetting behavior, a more complete crown can form and the sheet can slightly lift off the surface as can be seen, for example, in Fig. 15. At higher contact angles, the crown collapsed earlier leading to a slower spreading. In comparison with smooth surfaces,[24] the general influence of the wettability is lower with the exception of the crown splashing effect. The viscosity of the fluids shows the same tendency as for the smooth surfaces. An increasing viscosity usually decreases the absolute spreading diameter but increases the duration of the spreading process. Only for the lowest impact height, the higher viscosities also lead to larger spreading diameters. This behavior might be due to the lower inertial forces and is changing by increasing impact energy. The second finding stands here in contradiction to other literature findings of Rioboo *et al.*[2] but has been also found for the same experimental parameters with smooth surfaces.[24] However, their range and viscosity increment were by far larger than ours. A further analysis in the future with a fine increment in viscosity might be interesting in order to maybe show a turning point of the relationship between viscosity and spreading diameter. The influence of the surface topography, represented by the Wenzel factor r, onto the maximum spreading diameter is mostly negligible. A slight increase in spreading diameter might be assumed for finer pillar structures. In comparison with the pillars, the grooves show also a slightly increased maximum spreading diameter.

C. Impact regimes and splashing limit

Three impact regimes were identified: deposition, splashing, and rebound. Within these regimes, different cases were identified, deposition with and without fingering, prompt and crown splash, and partial

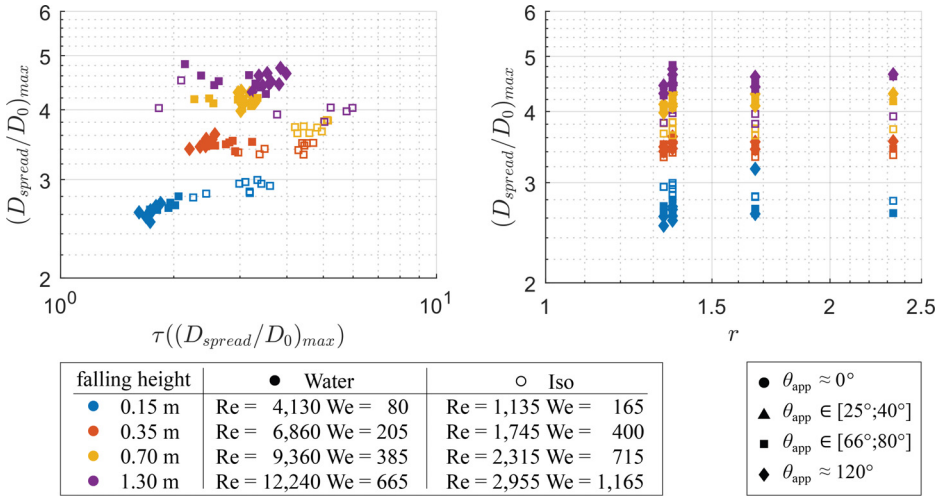

FIG. 5. Normalized droplet spreading diameter over the dimensionless time τ and the Wenzel factor r characterizing the surface topography type.

rebound. The surface topography of the surface samples and, consequently, their roughness was changed in order to identify its influence upon the splashing limit. In addition to that, the wettability was, independently of the structure pattern, modified using plasma activation and polymerization in order to assess also this influence on the splashing threshold.

In the following, existing correlations and approaches are compared and eventually modified to describe the splashing limit and to show the influence of surface roughness. At first, the splashing limit developed by Vander Wal *et al.*[8] for a droplet impact onto dry solid surfaces is considered. This is the splashing limit that best fitted the results of our previous studies onto dry smooth surfaces.[24] This correlation depends on the Ohnesorge number $Oh = \sqrt{We}/Re$ and the Reynolds number Re, Eq. (5). Considering this correlation, a modified K factor was investigated including the influence of the Wenzel factor r. The Wenzel factor r was used as influencing parameter since it is necessary to include the influence of surface micro-structures on the splashing limit. The existing equation was empirically changed to assess the influence of the surface roughness and the liquid properties. An influence of the apparent contact angle θ_{app} could not be found, so the splashing limit seems to be independent of the wettability in the here considered parameter range. This modified K factor changes from the original only by the exponent of the Ohnesorge number Oh, which includes the Wenzel factor r, as displayed in Eq. (6)

$$K_{crit} = OhRe^{0.609}\ (\text{Vander Wal } et\ al.^{8}), \tag{5}$$

$$K_{mod} = Oh^{1/(1.3\sqrt{r})}Re^{0.609}\ (\text{this article}). \tag{6}$$

Figure 6 shows how this boundary increases with an increase in the Wenzel factor. The critical K factor for smooth surfaces using the original correlation [Eq. (5)] is given in Eq. (7) and the proposed empirically found K_{mod} for the impact onto rough surfaces using the modified correlation [Eq. (6)] is reported in Eq. (8)

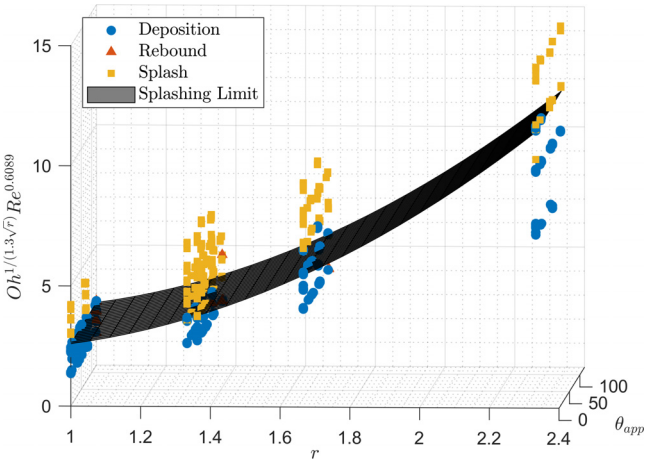

FIG. 6. Modified K-factor based on the original K-factor of Vander Wal *et al.*[8] over the roughness factor r introduced by Wenzel[29] and the apparent contact angle θ_{app}. The modified critical K-factor can be calculated from Eq. (8). A roughness factor of $r = 1$ corresponds to the results for the impact on smooth surfaces of the previous work.[24]

$$K_{crit} = 0.85\ (\text{Vander Wal } et\ al.^{8}), \tag{7}$$

$$K_{mod} = 3.5(r-1)^2 + 2(r-1) + 2.6\ (\text{this article}). \tag{8}$$

This equation was developed to describe properly the splashing limit, dependent on the surface Wenzel factor r. The small number of rebound cases did not make it possible to clearly define an individual limit for rebound cases. So, a correlation including this regime needs to be investigated in future works.

Roisman *et al.*[3] proposed a correlation for the splashing limit for the impact with rough surfaces. They determined that the parameters that mostly influence this type of impacts are the Weber number and the characteristic slope of the substrate morphology, which is defined by the ratio between the average height of the protruding peaks above the roughness profile and the mean width of a profile element, R_{pk}/R_{sm}. In their study, they only used surfaces with irregular roughness, while in this work only structures with regular roughness are studied. So, R_{pk} is difficult to define in our case since there are no protruding peaks on our structures with well-defined height.

Therefore, a geometrical approach was chosen to describe the splashing tendency on rough surfaces. As described before, Tsai *et al.*[19] reported that the arrangement of the pillars strongly influences the splashing outcomes. Hereby, the surface topography has been described in a two-dimensional way, which was not sufficient for our results. Thus, our splashing limit was formulated considering the Weber number and the modified parameter α_{mod} describing the surface topography in a three-dimensional way. Both parameters were found to be the most influencing ones, while the apparent contact angle had no effect on the splashing limit, see Fig. 7. Therefore, the critical Weber number We_{crit} for splashing depends only on α_{mod} and is given by Eq. (9),

$$We_{crit} = 30\left(\frac{b}{h}\right)^2 - 260\left(\frac{b}{h}\right) + 730. \tag{9}$$

According to this equation, the critical Weber number We_{crit} decreases with increasing α_{mod}. This is correct if we only consider the surface patterns composed of pillars with a square cross section with the spacing equal to the pillars width ($S2 - S4$).

Keeping the geometrical approach, different influencing parameters were considered in order to explain why the $S1$ surface is the one that promotes at most the formation of secondary atomization. It is known that the pillar height can promote or suppress droplet splashing.[21] However, in this study, all micro-structure patterns have the same height $h = 20\ \mu$m (Table I). Nevertheless, the results show that the relative height is decisive for the effect of splashing. Additionally, the droplet initial diameter should also be considered since the outcome could change depending on the ratio between droplet initial diameter and the structure size. A dimensionless parameter including pillar height h, droplet diameter D_0, and structure top area $w_1 w_2$ was studied: $hD_0/(w_1 w_2)$. Considering this dimensionless parameter, the splashing limit can be expressed as follows using empirically fitting of the data points inside the transition zone:

$$We_{crit} = 0.008\left(\frac{hD_0}{w_1 w_2}\right)^2 - 0.11\left(\frac{hD_0}{w_1 w_2}\right) + 180. \tag{10}$$

Figure 8 shows the splashing limit, which increases as $hD_0/(w_1 w_2)$ increases. $S1$ has the smallest $hD_0/(w_1 w_2)$, and it is the

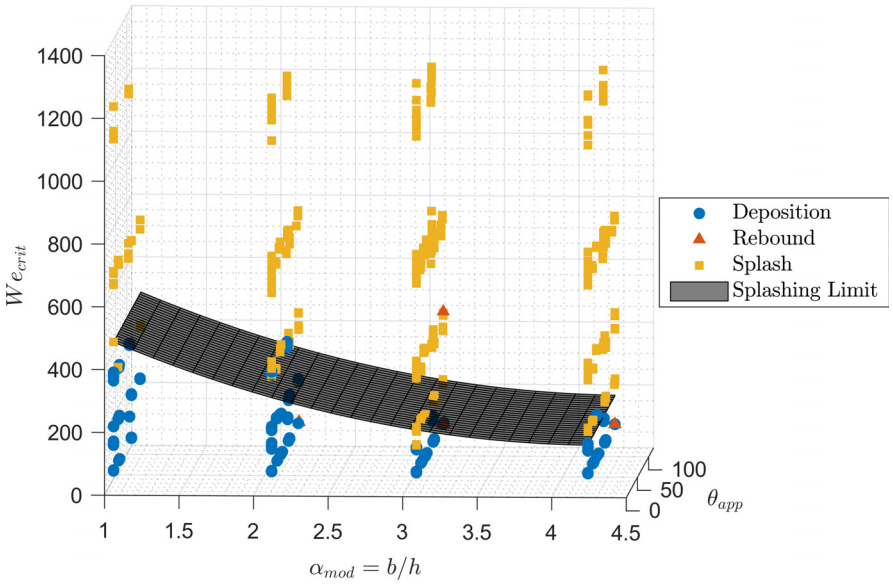

FIG. 7. Overview of impact outcomes using a modified parameter of Tsai *et al.*[19] extended by the apparent contact angle θ_{app}. α_{mod} was chosen as relation of the width of the junctions b and the height of the pillars, which can be both extracted from Table I for the respective surface types. The plane for the splashing limit (We_{crit}) can be described by Eq. (9).

structure pattern that promotes splashing the most. Considering the same D_0, S1 is the pattern that has the smallest relative height in comparison with the structure top area. As stated before, splashing is promoted by a smaller height,[21] which can explain why splashing is promoted by S1, followed by S2.

In summary, all three correlations are able to predict the splashing limit. The first introduced approach of Vander Wal *et al.*[8] is in very good agreement with the results for smooth surfaces. The modified correlation [Eq. (6)] is capable to predict the splashing limit for both smooth and rough surfaces. The second approach, originally proposed by Tsai *et al.*,[19] is focusing on the spacing between the roughness elements for regular micro-structured patterns. However, it could be shown that for the same mean roughness values and the same α-parameter different morphological outcomes can be obtained. Therefore, the three-dimensional α_{mod} has been introduced, which is assessing the geometric conditions in more detailed, and with its help, a correlation could be found for predicting the outcomes. Finally, the third approach considers a dimensionless parameter $hD_0/(w_1w_2)$, which relates three important factors, pillar height, droplet diameter, and structure top area. The height of the structures plays a role in the occurrence of splashing.[21] Although all patterns have the same pillar height $h = 20\ \mu$m, the relative height in comparison with the structure top area is smaller for S1, which is the structured pattern that better promotes splashing.

D. Morphological behavior: Qualitative analysis

This section provides a detailed description of droplet impact onto rough surfaces depending on the structure type, roughness scales, impact energy, fluid, and surface wettability. Within this parameter

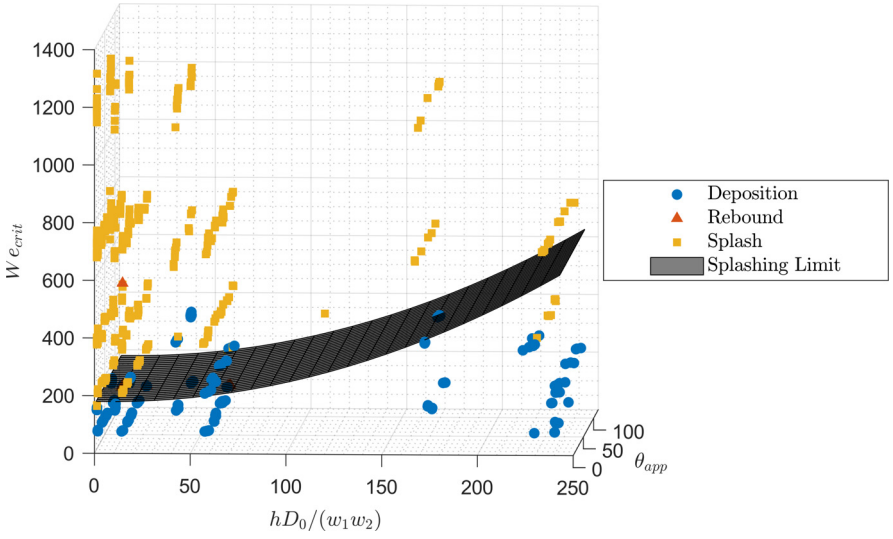

FIG. 8. Overview of impact outcomes using the dimensionless parameter $hD_0/(w_1w_2)$ extended by the apparent contact angle θ_{app}. This parameter relates the pillar height h, the droplet diameter D_0, and the structure top area w_1w_2. h, w_1, and w_2 can be extracted from Table I for the respective surface types. The plane for the splashing limit (We_{crit}) can be described by Eq. (10).

space, several phenomena were observed: deposition, fingering, prompt splash, crown splash, receding breakup, and partial rebound as well as heterogeneous wetting states. In the following, the focus is set to the heterogeneous wetting, while the macroscopic morphologies are mostly mentioned.

Figure 9 shows the regimes observed when a distilled water droplet impinges onto Lexan® (PC) and Plexiglas® (PMMA) micro-structured surfaces for different impact velocities and wettability behaviors. Additionally, its most significant features are also included to distinguish different spreading or receding behaviors within the same impact regime. For the impact using Lexan® surfaces, the four different micro-structured patterns were considered. However, for the impact onto Plexiglas® only three different patterns were considered: *S*1, *S*2, and *S*3. This was because the smallest pillars with a square cross section *S*4 were damaged by the fabrication process.

At lower impact energies, the dominant outcome is deposition, except for the hydrophobic wetting condition where partial rebound is observed. No receding is observed for the two most wettable conditions. However, by increasing the contact angle, a thick lamella spreads until its maximum diameter and then recedes inward. During receding, the lamella breaks due to the micro-structures producing receding breakup, which is also observed for the non-wetting condition.

An important phenomenon that arises is related to how the liquid film spreads and wets the surface. The bottom and top perspectives in Fig. 10 show an example where the liquid film cannot penetrate completely within the pillars and, therefore, only wet the top of the pillars in these areas. After a short period of time, $\tau = 2.72$, the fluid starts to enter some gaps and encircle some of the areas to complete the lamella perimeter. At the last frame, the perimeter of the lamella is well delimited, but inside there are still empty spots where the liquid is above the top of the pillars without entering the spaces between them since they are filled with air.

Omniphobic surfaces can maintain a heterogeneous wetting state even for fluids with low surface tension.[45] The heterogeneous wetting state takes place when the asperities of a rough surface topography can sustain air entrapped inside the grooves underneath the liquid film. Hensel *et al.*[45] used the term "intrinsic contact angle" for the well-known Young contact angle, $\theta_{Y,}$ which is one of the parameters that define the heterogeneous wetting state. For water, a thermodynamically stable heterogeneous state is reachable at a Young contact angle (θ_Y) high enough, typically larger than 90°, and an appropriate roughness. Fluids with lower surface tension than water can reach a heterogeneous wetting state at $\theta_Y < 90°$ even on low-energy surface materials. However, the heterogeneous wetting state is energetically metastable and can be transferred into a homogeneous wetting state by pressure fluctuations like acoustical or mechanical vibrations that would result in a poor resistance against wetting. Usually, for $\theta_Y < 20°$ the liquid instantaneously penetrates the cavities due to the continuously downward-directed capillary net force. We observed the heterogeneous wetting state for the partially wettable and non-wettable surfaces for both materials. A summary of the outcomes dependent on the impact parameters and surface properties is depicted in Fig. 11. Due to the increase in the hydrostatic pressure inside the cavity, the liquid–air interface falls into the cavity. There is a critical pressure difference to achieve a breakthrough scenario. Within this scenario, two phenomena are possible. The first one is the canthotaxis effect, where the critical pressure difference precisely corresponds to the geometrical boundary condition and is defined as

$$\Delta p_{break} = p_h - p_0 = \frac{2\gamma \sin(\theta_Y + \Psi)}{X}, \tag{11}$$

where p_h and p_0 are the hydrostatic and the air pressure, respectively; γ is the liquid surface tension; Ψ is the geometrical edge angle; and X is the distance between the three-phase contact line and the symmetry center of the cavity. The second phenomenon is the Laplace breakthrough where the liquid–air interface assumes a semicircular shape before it fills the cavity. The critical pressure difference is defined as follows:

$$\Delta p_{break} = p_h - p_0 = \frac{2\gamma}{X}. \tag{12}$$

In both phenomena, for the critical pressure difference calculation, the length scale in the denominator is *X,* which is in our case assumed to be *b* following the definition of Tsai *et al.*[19] Thus, the larger the *X* value, the smaller the pressure difference to fill the cavity. *S*2 has the highest *b* value, so it is the surface topography that demands the lowest pressure difference to reach the breakthrough pressure.

As mentioned, water droplet impact onto hydrophobic micro-structured surfaces results in partial rebound. Figure 12 shows an example of partial rebound for water droplet impact onto a hydrophobic Lexan® *S*4 micro-structured surface from three different perspectives: lateral, top, and bottom. At the moment of impact, from the bottom perspective, it is possible to see a dry zone around the impact site. Similar to Fig. 10, this bright spot corresponds to an area where the fluid did not enter the gaps within the structure due to a heterogeneous wetting state. As already mentioned and also reported in the literature,[46–48] when the droplet is approaching the target surface, it starts to flatten at the bottom. An air cushion can even be formed between the droplet and a micro-structured target surface at the moment of impact. For *S*3 and *S*4, a non-wetted central area is observed due to this air cushion that provided a heterogeneous wetting state, but for *S*1 and *S*2, only a bright small spot is seen at the impact point, suggesting just the formation of a small air bubble. After impact, a thick lamella is formed and spreads radially until reaching its maximum diameter at $\tau = 1.36$. Heterogeneous wetting states are observed for all micro-structured arrangements, see Fig. 11. After reaching the maximum spreading diameter, it quickly recedes inward ($\tau = 3.05$) forming a high central jet ($\tau = 8.15$) that breaks up and ejects large secondary droplets ($\tau = 13.24$). It is important to highlight that during the receding phase, receding breakup occurs but in a smaller magnitude than for the impact on partially wettable surfaces, $\theta_{app} \in [75°–80°]$. This fact can be linked to a higher receding velocity as a consequence of the lower tendency of liquid sticking to the surface, not allowing the breakup of the liquid lamella. The formation of a high central jet is promoted since less liquid is "lost" on receding breakup.

Increasing the impact energy promotes the occurrence of splashing. However, the surface pattern plays a role since prompt splash is observed for all wettability conditions but only for the impact with the surfaces composed of the largest structures. That can be justified by the splashing limit proposed in Eq. (10), where *S*1 presents the smallest relative height, so a higher tendency for splash formation. For the two most wettable conditions and the patterns composed of square pillars arranged in a square lattice, a new observed pattern called by the authors as "button effect" appears in the spreading lamella, see also Fig. 11. Figure 13 shows the pattern formed by four round areas

Water

		θ_{app} ≈0°	∈[25°-40°]	∈[75°-80°]	≈120°
We=80 Re=4130	PC	**Deposition** No receding		**Deposition** Recedes inwards Receding Breakup Heterogeneous wetting (S1, S3, S4)	**Partial Rebound** Quickly recedes Receding Breakup Heterogeneous wetting
	PMMA				**Partial Rebound** (S1, S2) **Deposition** (S3) Quickly recedes Receding Breakup Heterogeneous wetting
We=205 Re=6860	PC	**Prompt Splash** (S1, S2) **Deposition** (S3, S4) No receding Button Effect (PC: S2-S4)	**Prompt Splash** (S1, S2) **Deposition** (S2, S3, S4) No receding Button Effect (PC: S3, S4)	**Prompt Splash** (S1, S2) **Deposition** (S3, S4) Recedes inwards Receding Breakup Heterogeneous wetting	**Prompt Splash** (S1, S2, S3) **Deposition** (S3, S4) Quickly recedes Receding Breakup Heterogeneous wetting
	PMMA				**Partial Rebound** (S_1) **Prompt Splash** (S_1-S_3) **Deposition** (S_3) Quickly recedes Receding Breakup Heterogeneous wetting
We=385 Re=9360	PC	**Crown Splash** (S1) **Prompt Splash** **Deposition** (S4) No receding Button Effect (S2, S3, S4)		**Crown Splash** Quickly recedes Receding Breakup Heterogeneous wetting Button Effect (PC - S3, S4)	**Crown Splash** (S2, S3, S4) **Prompt Splash** Quickly recedes Receding Breakup Heterogeneous wetting Button Effect (S3, S4)
	PMMA	**Prompt Splash** No receding Heterogeneous wetting (S1)			**Partial Rebound** (S1) **Prompt Splash** Quickly recedes Receding Breakup Heterogeneous wetting
We=665 Re=12240	PC	**Crown Splash** No receding Button Effect (S3, S4)	**Crown Splash** (S1, S2, S3) **Prompt Splash** (S4) No receding Button Effect (S3, S4)	**Crown Splash** Quickly recedes Receding Breakup Heterogeneous wetting Button Effect (S3, S4)	
	PMMA	**Prompt Splash** No receding	**Crown Splash** (S1) **Prompt Splash** (S3, S4) No receding	**Crown Splash** Quickly recedes Receding Breakup Heterogeneous wetting	

FIG. 9. Description of the outcomes and its morphology depending on surface wettability and surface micro-structure pattern for PC and PMMA on the water droplet impact at different impact energies.

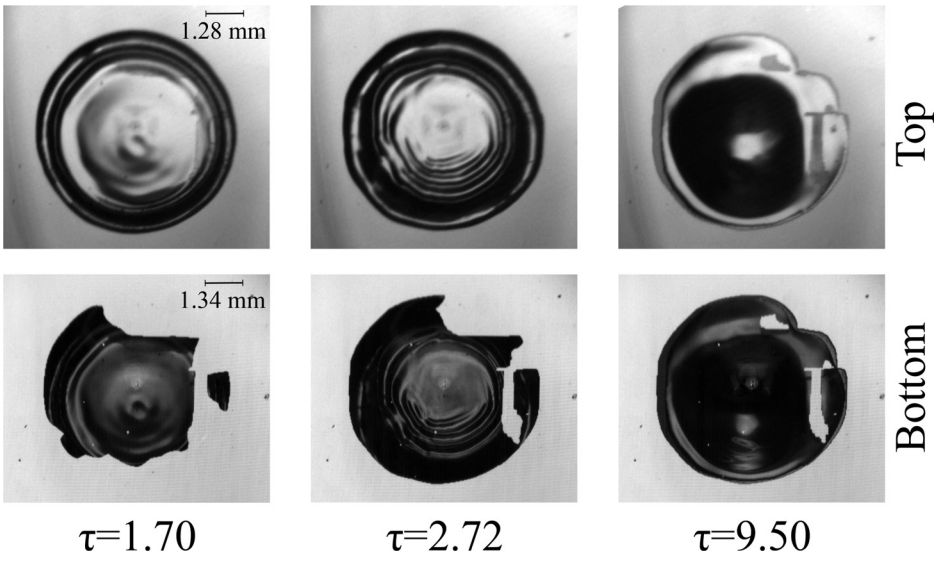

FIG. 10. Top and bottom views of non-wetted areas caused by heterogeneous wetting on a water droplet impact on a partially wettable *S4* Lexan® surface, $\theta_{app} \in [75°–80°]$, $We = 80$.

Wettability / Structure	Height	PC 0.15m	PC 0.35m	PC 0.70m	PC 1.30m	PMMA 0.15m	PMMA 0.35m	PMMA 0.70m	PMMA 1.30m
Water 0°	#4: 15µm		"Button effect"	"Button effect"	"Button effect"				
	#3: 30µm								
	#2: 60µm								
	#1: grooves.								
Water 25° to 40°	#4: 15µm		"Button effect"	"Button effect"	"Button effect"				
	#3: 30µm								
	#2: 60µm								
	#1: grooves.							Het. breakthr.	
Water 79.8° | 75.1°	#4: 15µm	Heterogeneous breakthrough	Heterogeneous breakthrough	"Button effect" & Het. break.	"Button effect" & Het. break.		Heterogeneous breakthrough	Heterogeneous breakthrough	Heterogeneous breakthrough
	#3: 30µm					Het. breakthr.			
	#2: 60µm			Heterogeneous breakthrough	Heterogeneous breakthrough				
	#1: grooves.	Het. breakthr.				Het. breakthr.			
Water 117° to 122°	#4: 15µm	Heterogeneous breakthrough	Heterogeneous breakthrough	"Button effect" & Het. break.	"Button effect" & Het. break.	Heterogeneous breakthrough	Heterogeneous breakthrough	Heterogeneous breakthrough	Heterogeneous breakthrough
	#3: 30µm								
	#2: 60µm			Heterogeneous breakthrough	Heterogeneous breakthrough				
	#1: grooves.								
Iso 0°	#4: 15µm		"Button effect"	"Button effect"	"Button effect"				
	#3: 30µm						"Button effect"		
	#2: 60µm						Heterogeneous breakthrough		
	#1: grooves.								
Iso 66° to 73°	#4: 15µm	Heterogeneous breakthrough	"Button" & "Cookie eff." & Het. break.	"Button" & "Cookie eff." & Het. break.	"Button" & "Cookie eff." & Het. break.				
	#3: 30µm					Heterogeneous breakthrough	"Button" & "Cookie eff." & Het. break.	"Button" & "Cookie eff." & Het. break.	"Button" & "Cookie eff." & Het. break.
	#2: 60µm		Heterogeneous breakthrough	"Button effect" & Het. break.	"Cookie eff." & Het. break.		Heterogeneous breakthrough	"Button effect" & Het. break.	
	#1: grooves.	Heterogeneous breakthrough		Heterogeneous breakthrough	"Cookie eff." & Het. break.	Heterogeneous breakthrough		"Cookie eff." & Het. break.	"Cookie eff." & Het. break.

FIG. 11. Regime map for heterogeneous wetting states dependent on the impact parameters and surface properties.

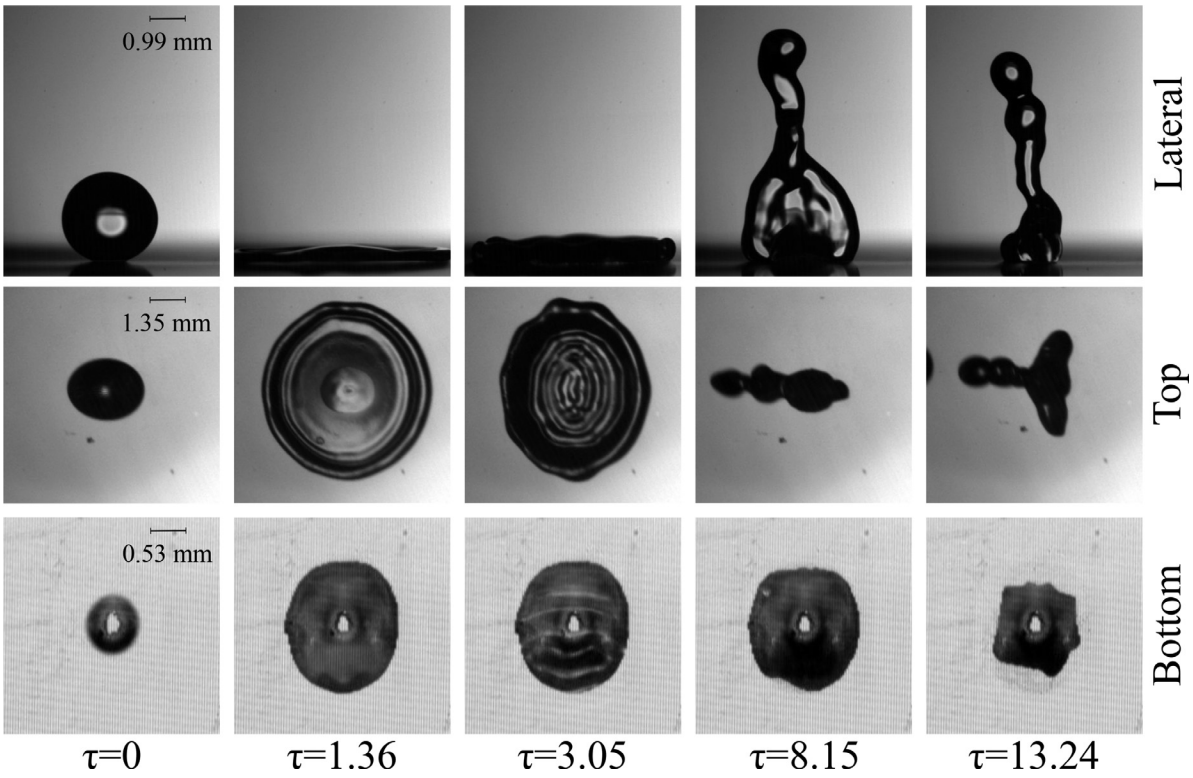

FIG. 12. Partial rebound of a water droplet onto a hydrophobic *S*4 Lexan® micro-structured surface for *We* = 80 from three different perspectives: lateral, top, and bottom.

centered at the impact point, where the concentration of tiny air bubbles seems to be higher. The mechanism of the button effect is based on the complete wicking of liquid inside the structure. Thus, small bubbles are trapped at the edges inside the structure and transported outward by the spreading movement of the droplet. Chandra and Avedisian[46] reported similar structures as "cellular structures," however for a completely different case. Their studies were carried out on heated stainless steel smooth walls, and these structures were formed

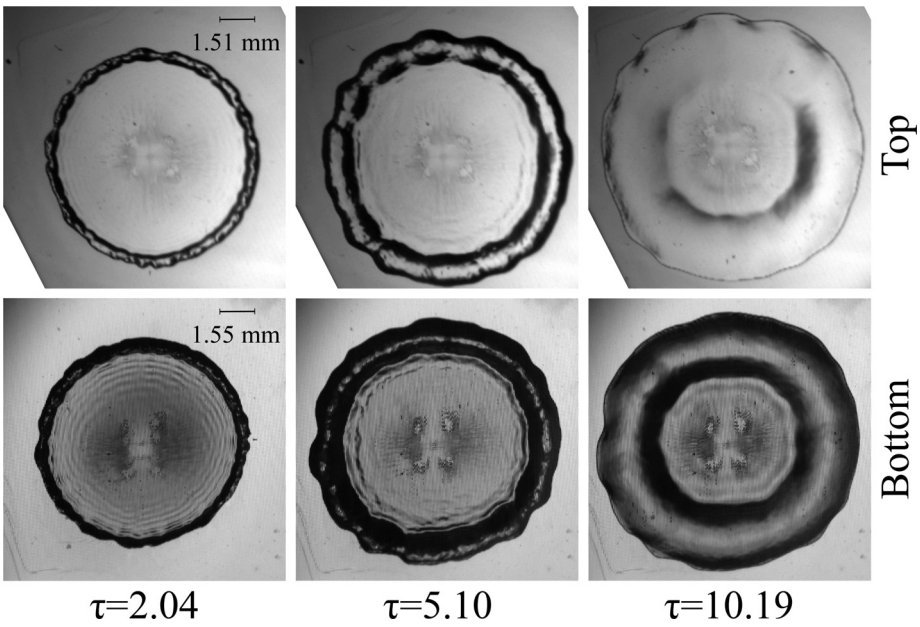

FIG. 13. Button effect from the top and bottom perspectives for a water droplet impact onto a fully wettable *S*3 Lexan® surface for *We* = 205.

due to the interaction of heptane droplets with the heated wall. Therefore, it is questionable if the same mechanisms are behind both observations. On the other hand, this type of fourfold symmetry was also addressed in the literature[21,49,50] for the same arrangement of square pillars due to droplets ejected along the diagonal directions during prompt splash. Here, prompt splash is always a directional splashing following the orientation of the pillars/grooves.

Increasing the impact energy to $We = 385$, due to the formation of a weak and incomplete crown, crown splash is observed for all wettability behaviors. Here, the occurrence of a crown splash seems to be dependent on the combination of micro-structured pattern and wettability behavior, as can be seen in Fig. 9. Keeping the impact energy at $We = 385$, the only event of deposition is for *S*4, which is the surface pattern with larger relative height in comparison with the structure top area [see Eq. (10) and Fig. 8]. This is also the surface with the smallest structures and with the smallest interspace between pillars. According to Xu,[21] increasing pillar spacing enhances the characteristic decay length promoting splashing. A reason for this behavior might also be that the impact energy is partially dissipating inside the structures and is not sufficiently available to enable splashing. At this impact energy, there is still an event of partial rebound on the impact with *S*1 hydrophobic PMMA. This phenomenon is possible due to the larger extend of the central jet, which allows its breakup and consequent ejection of droplets. Regarding the fact that *S*1 is the only structure without crown splashing for the impact onto Lexan® surfaces, a possible explanation could be based on the higher magnitude of prompt splash, which could be inhibiting the crown-like sheet formation. The energy for the crown sheet formation might have been splashed away already during the prompt splash event. Other characteristics, like the button effect and the heterogeneous wetting state, are present for similar conditions as the ones at a lower height.

At the highest impact energy, the dominant phenomenon is crown splash. The crown is complete due to the excess of impact energy. Crown splash is promoted by the surfaces composed of the largest micro-structures as described by Eq. (10). For high contact angles, after the maximum spreading diameter, a receding phase follows, creating central jets, but for none of the cases partial rebound occurred. An important remark of this study on the impact on micro-structured surfaces is the fact that while increasing impact energy the tendency to produce partial rebound does not increase as it usually does on the impact with smooth surfaces.[51] On smooth surfaces, the increase in impact energy increases the receding velocity, increasing the height of the central jet and consequently promoting its breakup and the ejection of secondary droplets. In previous works[24] on smooth surfaces, the tendency for rebound increased with the impact energy until a certain value in which the receding breakup was so strong that it did not allow the formation of a central jet. However, for similar impact conditions, there were still rebound events on the smooth surfaces. In this study, rebound is promoted for the impact with lower impact energies. On rough surfaces, the increase in receding velocity also promotes an increase in receding breakup due to the discontinuities at the liquid–solid interface. So, there is no fluid left to form this high central jet and that is why for high impact energies the partial rebound is suppressed.

Figure 14 summarizes the outcomes obtained for the different impact conditions and the main characteristics with isopropanol. At low impact energy, deposition and prompt splash are observed. With increasing energy, a combination of directional prompt and directional crown splash can be observed as shown in Fig. 15. Here, the crown forms an incomplete crown sheet parallel to the grooves length. As shown for $\tau = 0.30$, directional prompt splash is formed parallel to the grooves length and a tiny crown sheet begins to form sideways ($\tau = 0.48$). This liquid sheet evolves and, shortly after, it breaks ejecting secondary droplets ($\tau = 0.73$).

A heterogeneous wetting state is observed on the impact with partial wetting surfaces, see Fig. 11. However, increasing the impact energy for the lower wettability $\theta_{app} \in [66°–73°]$ and the surfaces with a higher Wenzel factor *r*, *S*3 and *S*4, a peculiarity denoted by the authors as "cookie effect" was identified for both materials, see Fig. 16. The heterogeneous wetting state left round areas where the fluid cannot enter the gaps within the structures and then the fluid on top of the pillars circumvents these areas and creates "empty" zones where there is no fluid ($\tau = 12.09$). For *S*3 and *S*4, the liquid lamella has plenty of these "holes" reminding of a cookie. In addition, the formation mechanism of these two unilateral fingers formed on one side of the lamella should be investigated in future works.

Increasing further the impact energy enhances the occurrence of prompt and crown splash. At $We = 715$, the impact onto the micro-structured arrangements *S*3 and *S*4 tends to originate prompt splash. However, as displayed in Fig. 8, surfaces with a smaller top area $w_1 w_2$ demand a higher impact energy resulting in a larger We_{crit}, respectively, to produce prompt splashing as well as for a crown-sheet formation. Additionally, they have a smaller interspace *b* and energy might dissipate more in these cases not allowing the formation of a crown sheet. On the other hand, there is only one event of prompt splash for *S*1. This shows that a stronger prompt splash can suppress the crown sheet formation. The crown formation at this impact energy slightly depends on specific conditions regarding the impact point of the droplet, which suggests that this is a transition zone between both phenomena. There is a heterogeneous wetting state similar to the one reported for the lower impact height, as well as the formation of a cookie effect and a button effect for the surfaces with higher Wenzel factors, see Fig. 11.

For the highest falling height, the impact energy is high enough to allow the effect of the micro-structured patterns to not be distinguishable anymore, producing the same outcomes with the same characteristics independent of the size or arrangement of the pillars. Crown splash was the outcome for all cases and all wettabilities.

E. Conclusions

Droplet impact upon micro-structured surfaces is far from being fully understood. In this work, distilled water and isopropanol droplets impinging on Lexan® and Plexiglas® surfaces with different micro-structured patterns and wettability behavior ($0° < \theta_{app} < 120°$) have been investigated. Three different perspectives of the phenomena were captured including a bottom perspective in a total internal reflection configuration, which is, to the authors' knowledge, only very rare in the literature[24] so far. From this perspective, it is possible to observe different wetting states due to the transparency of the polymeric surface samples. Four different surface micro-structures, characterized by different length scales, were considered. Furthermore, the wettability of the surface samples was altered by using plasma activation and plasma polymerization processes. This is one of the novelties of this

Isopropanol

		θ_{app} ≈0°		∈[66°-73°]	
We=165 Re=1135	PC	**Prompt Splash** (S1) **Deposition** No receding		**Prompt Splash** (S1) **Deposition** Recedes inwards Heterogeneous wetting (S1, S3, S4)	
	PMMA	**Deposition** No receding			
We=400 Re=1745	PC	**Crown Splash** (S1) **Prompt Splash** (S2, S3) **Deposition** (S3, S4) No receding Button Effect (S3, S4)		**Prompt Splash** (S1, S2) **Deposition** (S3, S4) Barely recedes Heterogeneous wetting Button Effect (S3, S4) Cookie Effect (S3, S4)	
	PMMA	**Prompt Splash** **Deposition** (S3) No receding Button Effect (S3)			
We=715 Re=2315	PC	**Crown Splash** (S1, S2) **Prompt Splash** (S3, S4) No receding Button Effect (S3, S4)		**Crown Splash** (S1, S2, S3) **Prompt Splash** (S4) Barely recedes Heterogeneous wetting Button Effect (S2, S3, S4) Cookie Effect (S1, S3, S4)	
	PMMA	**Crown Splash** (S2, S3) **Prompt Splash** (S1) No receding			
We=1165 Re=2955	PC	**Crown Splash** No receding Button Effect (PC - S3, S4)		**Crown Splash** No receding Heterogeneous wetting Button Effect (S2, S3, S4) Cookie Effect	
	PMMA				

FIG. 14. Description of the outcomes and its morphology depending on surface wettability and surface micro-structure pattern for PC and PMMA on the isopropanol droplet impact at different impact energies.

study, since it allowed us to change the wettability without changing the surface material or roughness.

The results were primarily divided into three main impact regimes: deposition, splashing, and rebound. However, it is difficult to define one generalized splashing limit for rough surfaces, while the surface wettability does not seem to have a significant influence on the limit. Different approaches had been discussed and modified in order to define the splashing limit that fits the results of this study. The correlation developed by Vander Wal *et al.*[8] had to be modified using the Wenzel factor[29] r and can now predict a splashing limit for smooth and rough surfaces. The approach of Tsai *et al.*,[19] who investigated the pillar arrangement, was extended to consider the three-dimensional geometry of the interspaces and can then describe the splashing limit very well for the surface patterns composed of pillars with a square cross section. A new geometrical approach is proposed considering the dimensionless parameter $hD_0/(w_1w_2)$, which defines the relative height considering the droplet diameter and the structure top area. A smaller relative height implies a smaller critical Weber number for splash formation.

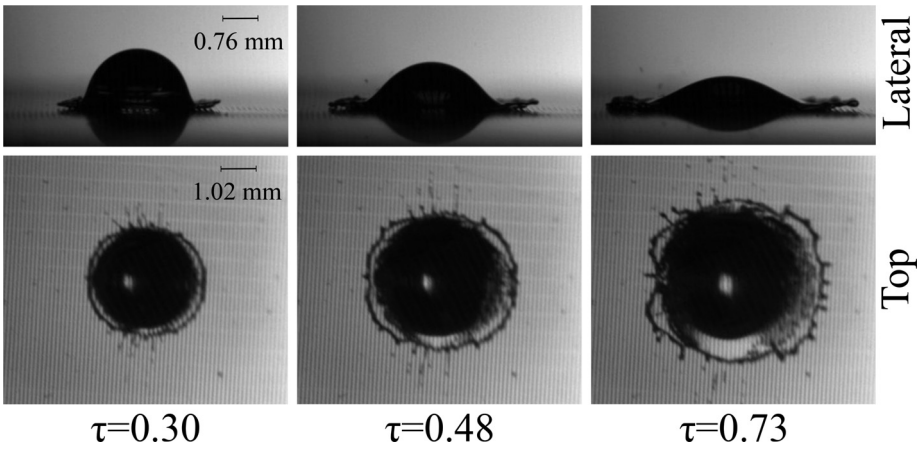

FIG. 15. Directional prompt splash and crown splash with an incomplete crown for the isopropanol droplet impact onto a fully wettable ($\theta_{app} \approx 0^\circ$) *S*1 Lexan® surface, $We = 400$.

In the following, the main findings for the impact morphology of the impact onto the micro-structures are summarized. Considering distilled water, deposition is the outcome for the lowest impact energy. On the hydrophobic experiments, partial rebound was formed due to the wide receding and consequent formation of a high central jet. Increasing the impact energy, directional prompt splash appears for the surface patterns with larger micro-structures. Increasing further the impact energy promotes directional prompt splash, even for the smaller surface structures, which seem to inhibit splashing. The smaller the surface structures are, the more impact energy seems to dissipate, which is then not available for creating a splash. A crown splash forms at the two highest impact energies, depending also on the structure type but not on the wettability. The receding phase is promoted by lower wettabilities since surface tension is pulling the fluid back again. For hydrophobic surfaces, by increasing impact energy, the droplet lamella is spreading more and the thickness is consequently decreasing. Therefore, the perturbations of the surface discontinuities are increasing until it comes to receding breakup, although the receding velocity is increasing. As a consequence, less fluid is available to form a central jet, inhibiting partial rebound.

Splashing is promoted by liquids with low surface tension. Impacts of isopropanol result in weak, directional splashing for the largest structures (*S*1), even for the lowest impact energy. Increasing the impact energy increases the probability to obtain prompt splash and also promotes crown splash. For too high impact energies, the effect of the micro-structured patterns is not distinguishable anymore due to the dominant inertia forces, producing the same outcomes and characteristics independent of the size or arrangement of the pillars.

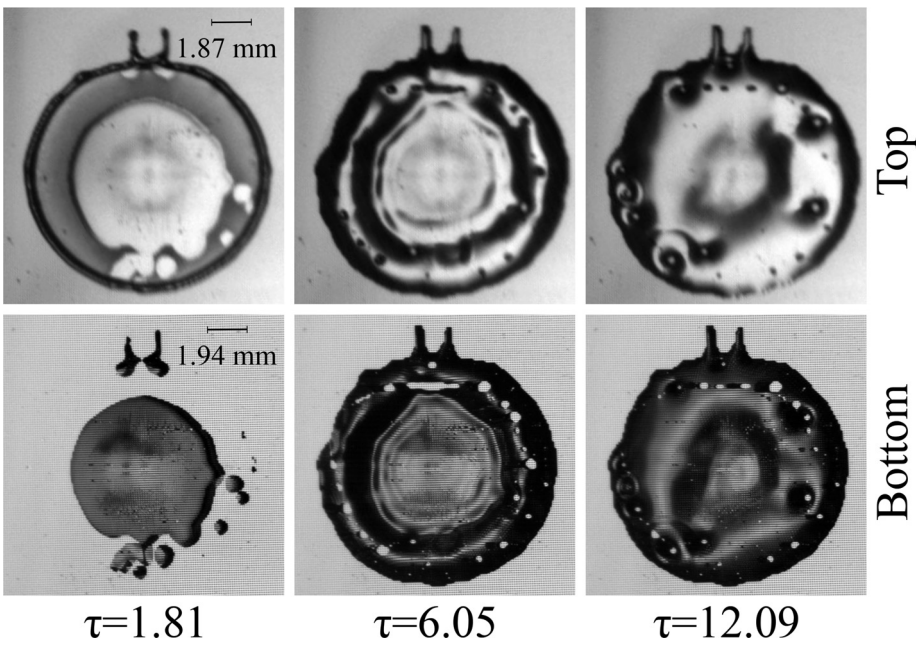

FIG. 16. Cookie effect seen from the top and bottom perspectives for the isopropanol droplet impact onto a *S*3 Plexiglas® surface with $\theta_{app} \in [66^\circ\text{–}73^\circ]$, $We = 400$.

As mentioned, the three different perspectives were very important to understand all morphological features of the impact. From the bottom perspective, it was observed that the micro-structures promote the formation of several air bubbles contrarily to smooth surfaces[24] where only one air bubble is formed. Further, the button effect was an important characteristic mainly on the impact onto Lexan® surfaces with micro-structures composed of pillars with a square cross section resulting in four round areas crowded with small air bubbles near the impact site.

Heterogeneous wetting states, where air is sustained inside the gaps underneath the liquid film, were mainly promoted by high contact angles and low interspaces. Very large non-wetted areas are formed at the impact area due to the formation of an air cushion for the impact on hydrophobic samples with high roughness factors *r*. Another effect noticed exclusively for isopropanol droplets is the cookie effect, where several round areas remain non-wetted within the liquid lamella.

ACKNOWLEDGMENTS

The authors kindly acknowledge the financial support of this work by the Deutsche Forschungsgemeinschaft (DFG) in the frame of the International Research Training Group "Droplet Interaction Technologies" (*GRK 2160: DROPIT*) under the Project No. 270852890. Additionally, the authors would like to acknowledge the support of Fundação para a Ciência e a Tecnologia (FCT) through the Ph.D. Scholarship No. SFRH/BD/140009/2018 and the Project No. UIDB/50022/2020. The mold fabrication, the surface replication, and the SEM analysis were carried out with the support of the Karlsruhe Nano Micro Facility (KNMF Proposal No. 2016-017-016369, www.knmf.kit.edu) and a Helmholtz Research Infrastructure at Karlsruhe Institute of Technology (KIT, www.kit.edu).

AUTHOR DECLARATIONS

Conflict of Interest

The authors have no conflicts to disclose.

Author Contributions

Patrick Foltyn: Conceptualization (equal); Data curation (equal); Formal analysis (equal); Investigation (equal); Methodology (equal); Validation (equal); Visualization (equal); Writing – original draft (equal). **Daniela Filipa Santo Ribeiro:** Data curation (equal); Formal analysis (equal); Investigation (equal); Validation (equal); Visualization (equal); Writing – original draft (equal). **André Resende Rodrigues Silva:** Funding acquisition (equal); Investigation (supporting); Project administration (supporting); Writing – review & editing (equal). **Grazia Lamanna:** Funding acquisition (supporting); Investigation (supporting); Project administration (supporting); Writing – review & editing (equal). **Bernhard Weigand:** Funding acquisition (lead); Project administration (lead); Resources (equal); Writing – review & editing (equal).

DATA AVAILABILITY

The data that support the findings of this study are available from the corresponding author upon reasonable request.

REFERENCES

[1]A. L. Yarin, I. V. Roisman, and C. Tropea, "Drop impact onto dry surfaces with complex morphology," in *Collision Phenomena in Liquids and Solids* (Cambridge University Press, 2017), pp. 155–252.
[2]R. Rioboo, M. Marengo, and C. Tropea, "Time evolution of liquid drop impact onto solid, dry surfaces," Exp. Fluids **33**, 112–124 (2002).
[3]I. V. Roisman, A. Lembach, and C. Tropea, "Drop splashing induced by target roughness and porosity: The size plays no role," Adv. Colloid Interface Sci. **222**, 615–621 (2015).
[4]R. L. Vander Wal, G. M. Berger, and S. D. Mozes, "The combined influence of a rough surface and thin fluid film upon the splashing threshold and splash dynamics of a droplet impacting onto them," Exp. Fluids **40**, 23–32 (2006).
[5]C. Bai and A. D. Gosman, "Development of methodology for spray impingement simulation," in *International Congress and Exposition* (SAE International, 1995).
[6]C. Josserand, L. Lemoyne, R. Troeger, and S. Zaleski, "Droplet impact on a dry surface: Triggering the splash with a small obstacle," J. Fluid Mech. **524**, 47–56 (2005).
[7]C. Mundo, M. Sommerfeld, and C. Tropea, "Droplet-wall collisions: Experimental studies of the deformation and breakup process," Int. J. Multiphase Flow **21**, 151–173 (1995).
[8]R. L. Vander Wal, G. M. Berger, and S. D. Mozes, "The splash/non-splash boundary upon a dry surface and thin fluid film," Exp. Fluids **40**, 53–59 (2006).
[9]C. Antonini, A. Amirfazli, and M. Marengo, "Drop impact and wettability: From hydrophilic to superhydrophobic surfaces," Phys. Fluids **24**, 102104 (2012).
[10]C. D. Stow and M. G. Hadfield, "An experimental investigation of fluid flow resulting from the impact of a water drop with an unyielding dry surface," Proc. R. Soc. London, Ser. A **373**, 419–441 (1981).
[11]K. Range and F. Feuillebois, "Influence of surface roughness on liquid drop impact," J. Colloid Interface Sci. **203**, 16–30 (1998).
[12]E. Papierowska, R. Mazur, T. Stańczyk, M. Beczek, J. Szewińska, A. Sochan, M. Ryżak, J. Szatyłowicz, and A. Bieganowski, "Influence of leaf surface wettability on the drop splash phenomenon," Agric. Meteorol. **279**, 107762 (2019).
[13]J. Shen and X. Wang, "Substrate counts: Quantitative effects of surface roughness on fingering pattern and rim shape of an impacting drop," Phys. Fluids **32**, 093313 (2020).
[14]T. de Goede, K. de Bruin, N. Shahidzadeh, and D. Bonn, "Droplet splashing on rough surfaces," Phys. Rev. Fluids **6**, 043604 (2021).
[15]D. Sivakumar, K. Katagiri, T. Sato, and H. Nishiyama, "Spreading behavior of an impacting drop on a structured rough surface," Phys. Fluids **17**, 100608 (2005).
[16]V. Vaikuntanathan and D. Sivakumar, "Maximum spreading of liquid drops impacting on groove-textured surfaces: Effect of surface texture," Langmuir **32**, 2399–2409 (2016).
[17]S. Yada, B. Allais, W. van der Wijngaart, F. Lundell, G. Amberg, and S. Bagheri, "Droplet impact on surfaces with asymmetric microscopic features," Langmuir **37**, 10849–10858 (2021).
[18]W. Ding, C. A. Dorao, and M. Fernandino, "Anisotropic wetting and final shape of droplets impacting on micropillars with non-vertical lateral walls," AIP Adv. **11**, 115319 (2021).
[19]P. Tsai, R. C. A. van der Veen, M. van de Raa, and D. Lohse, "How micropatterns and air pressure affect splashing on surfaces," Langmuir **26**, 16090–16095 (2010).
[20]W. Ren, P. Foltyn, A. Geppert, and B. Weigand, "Air entrapment and bubble formation during droplet impact onto a single cubic pillar," Sci. Rep. **11**, 18018 (2021).
[21]L. Xu, "Liquid drop splashing on smooth, rough, and textured surfaces," Phys. Rev. E **75**, 056316 (2007).
[22]B. A. Malouin, N. A. Koratkar, A. H. Hirsa, and Z. Wang, "Directed rebounding of droplets by microscale surface roughness gradients," Appl. Phys. Lett. **96**, 234103 (2010).
[23]S. Yada, U. Lacis, W. van der Wijngaart, F. Lundell, G. Amberg, and S. Bagheri, "Droplet impact on asymmetric hydrophobic microstructures," Langmuir **38**, 7956–7964 (2022).

[24]P. Foltyn, D. Ribeiro, A. Silva, G. Lamanna, and B. Weigand, "Influence of wetting behavior on the morphology of droplet impacts onto dry smooth surfaces," Phys. Fluids **33**, 063305 (2021).
[25]A. Karl, J. Wolber, and A. Frohn, "Interaction of droplet groups with hot walls above the Leidenfrost-temperature," in *Proceedings of the 13th International Conference on Liquid Atomization Spray System* (ILASS, 1997), Vol. 13, pp. 458–464.
[26]N. Roth, A. Karl, and A. Frohn, "Observation of liquid-wall contact during droplet impact," in *Proceedings of the 14th International Conference on Liquid Atomization Spray System* (ILASS, 1998), Vol. 14, pp. 103–107.
[27]N. R. Arnold Frohn, *Dynamics of Droplets* (Springer, Berlin, Heidelberg, 2000).
[28]L. P. Yarin, *The Pi-Theorem: Applications to Fluid Mechanics and Heat and Mass Transfer*, Experimental Fluid Mechanics, Vol. 1 (Springer-Verlag GmbH, Berlin, 2012).
[29]R. W. Wenzel, "Resistance of solid surfaces to wetting by water," Ind. Eng. Chem. **28**, 988–994 (1936).
[30]P. Foltyn, M. Guttmann, M. Schneider, S. Fest-Santini, D. Wildenschild, and B. Weigand, "Fabrication and evaluation methods of micro-structured surfaces for droplet impact experiments," in *Droplet Interactions and Spray Processes*, edited by G. Lamanna, S. Tonini, G. E. Cossali, and B. Weigand (Springer International Publishing, Cham, 2020), pp. 71–86.
[31]P. Foltyn, F. Restle, M. Wissmann, S. Hengsbach, and B. Weigand, "The effect of patterned micro-structure on the apparent contact angle and three-dimensional contact line," Fluids **6**, 92 (2021).
[32]M. A. van Limbeek, M. Shirota, P. Sleutel, C. Sun, A. Prosperetti, and D. Lohse, "Vapour cooling of poorly conducting hot substrates increases the dynamic Leidenfrost temperature," Int. J. Heat Mass Transfer **97**, 101–109 (2016).
[33]*Optik*, 3rd ed., edited by E. Hecht (Addison-Wesley, Bonn, 1994), pp. X, 717.
[34]W. Wagner and A. Pruß, "The IAPWS formulation 1995 for the thermodynamic properties of ordinary water substance for general and scientific use," J. Phys. Chem. Ref. Data **31**, 387–535 (2002).
[35]J. R. Rumble, "Density rho at the temperature in c indicated by superscript," in *CRC Handbook of Chemistry and Physics* (CRC Press, 2019).
[36]IAPWS, "Revised release on surface tension of ordinary water substance," Technical Report No. R1-76, International Association for the Properties of Water and Steam, 2014.
[37]J. R. Rumble, "Viscosity of liquids as a function of temperature," in *CRC Handbook of Chemistry and Physics* (CRC Press, 2019).
[38]M. L. Huber, R. A. Perkins, A. Laesecke, D. G. Friend, J. V. Sengers, M. J. Assael, IN. Metaxa, E. Vogel, R. Mareš, and K. Miyagawa, "New international formulation for the viscosity of H_2O," J. Phys. Chem. Ref. Data **38**, 101–125 (2009).
[39]J. R. Rumble, "Surface tension at various temperatures," in *CRC Handbook of Chemistry and Physics* (CRC Press, 2019).
[40]P. Foltyn, A. Schlottke, and B. Weigand, "Effect of plasma activation on the contact angle of smooth polymer surfaces and its long-term durability in ambient air," in *10th International Colloids Conference, 7–9 December 2020 (Online) Palma de Mallorca, Spain* (Elsevier, 2020), Vol. 10.
[41]A. S. H. Moita and A. L. N. Moreira, "Influence of surface properties on the dynamic behavior of impacting droplets," in *Proceedings in 9th ICLASS—Europe* (Institute for Liquid Atomization and Spray Systems, Sorrento, Italy, 2003).
[42]Q. Wang, X. Lin, Y. Lin, J. Ma, J. Xiao, Y. Wu, and J. Wang, "Effects of surface roughness on splashing characteristics of large droplets with digital inline holographic imaging," Cold Regions Sci. Technol. **191**, 103373 (2021).
[43]L. Courbin, J. C. Bird, and H. A. Stone, "Splash and anti-splash: Observation and design," Chaos **16**, 041102 (2006).
[44]M. Pasandideh-Fard, Y. M. Qiao, S. Chandra, and J. Mostaghimi, "Capillary effects during droplet impact on a solid surface," Phys. Fluids **8**, 650–659 (1996).
[45]R. Hensel, R. Helbig, S. Aland, H. Braun, A. Voigt, C. Neinhuis, and C. Werner, "Wetting resistance at its topographical limit: The benefit of mushroom and serif t structures," Langmuir **29**, 1100–1112 (2013).
[46]S. Chandra and C. T. Avedisian, "On the collision of a droplet with a solid surface," Proc. R. Soc. London A **432**, 13–41 (1991).
[47]V. Mehdi-Nejad, J. Mostaghimi, and S. Chandra, "Air bubble entrapment under an impacting droplet," Phys. Fluids **15**, 173–183 (2003).
[48]D. B. van Dam and C. L. Clerc, "Experimental study of the impact of an ink-jet printed droplet on a solid substrate," Phys. Fluids **16**, 3403–3414 (2004).
[49]M. Reyssat, D. Richard, C. Clanet, and D. Quéré, "Dynamical superhydrophobicity," Faraday Discuss. **146**, 19–33 (2010).
[50]D. Bartolo, F. Bouamrirene, E. Verneuil, A. Buguin, P. Silberzan, and S. Moulinet, "Bouncing or sticky droplets: Impalement transitions on superhydrophobic micropatterned surfaces," Europhys. Lett. **74**(1209), 299–210 (2006).
[51]A. Moreira, A. Moita, and M. Panão, "Advances and challenges in explaining fuel spray impingement: How much of single droplet impact research is useful?," Prog. Energy Combust. Sci. **36**, 554–580 (2010).